Structural and Electronic Properties of PTCDA Thin Films on Epitaxial Graphene

Han Huang,[†] Shi Chen,[†] Xingyu Gao,[†] Wei Chen,[†,‡,*] and Andrew Thye Shen Wee[†,*]

[†]Department of Physics, National University of Singapore, 2 Science Drive 3, 117542 Singapore, and [‡]Department of Chemistry, National University of Singapore, 3 Science Drive 3, 117543 Singapore

ABSTRACT *In situ* low-temperature scanning tunneling microscopy is used to study the growth of 3,4,9,10-perylene tetracarboxylic dianhydride (PTCDA) on epitaxial graphene (EG) on 6H-SiC(0001), as well as on HOPG for comparison. PTCDA adopts a layer-by-layer growth mode, with its molecular plane lying flat on both surfaces. The PTCDA films grow continuously over the EG step edges, but not on HOPG. STS performed on single-layer PTCDA on monolayer EG shows a wide band gap larger than 3.3 eV, consistent with pristine PTCDA films. Synchrotron-based high-resolution photoemission spectroscopy reveals weak charge transfer between PTCDA and EG. This suggests weak electronic coupling between PTCDA and the underlying EG layer.

KEYWORDS: epitaxial graphene · silicon carbide · PTCDA · scanning tunneling microscopy · photoemission spectroscopy

Graphene, a single sheet of sp^2-bonded carbon arranged in a honeycomb lattice, has become a hot topic due to its unusual electronic properties which originate from the linear dispersion of its π and π^* bands in the vicinity of the K point in the hexagonal Brillouin zone.[1] Graphene represents the ideal two-dimensional electron gas system and has potential applications in high-speed, ballistic-transport-based electronic devices.[2,3] Epitaxial graphene (EG) on SiC has been demonstrated as a possible platform for the development of graphene-based electronics.[4−6] In order to use EG for electronic devices such as field-effect transistors (FETs), it is necessary to precisely control the charge carrier type and concentration in EG. Recently, there have been many experimental reports on doping graphene by adsorbates such as NH_3,[7] NO_2, H_2O molecules,[8,9] Bi, Sn, and Au atoms,[10] as well as organic molecules.[11−13] However, how to fabricate a buffer layer at atomic-scale to further build graphene-based nanoscale devices is less studied.

Because of the inertness of the graphene surface, it is very challenging to grow high-quality oxide thin films on graphene for top-gating FETs. Recently, Dai's group demonstrated that reactive sites on mechanically exfoliated graphene for atomic layer deposition of Al_2O_3 can be created by functionalization using the carboxylic acid derivative of PTCDA.[14] Therefore, it is necessary to understand the PTCDA film growth mechanism to fabricate pinhole-free PTCDA layers on graphene for the development of high-quality gate oxide films on top. Liu's group showed that high-performance bottom-contact organic field-effect transistors can be achieved using patterned graphene as source/drain electrodes.[15] In order to better optimize the device performance, we need to understand the interface electronic structures and energy level alignments between graphene electrode and organic thin films. PTCDA, whose molecular structure is shown in Figure 1a, has been extensively investigated as a model system for organic−inorganic interfaces and forms ordered structures on various substrates.[16−23] A scanning tunneling microscopy/spectroscopy (STM/STS) study on PTCDA on bilayer EG at 4.7 K reveals that PTCDA adopts non-planar adsorption geometry in a brick-wall structure, resulting in n-type doping of EG.[24] In contrast, another STM/STS investigation at room temperature suggests that PTCDA forms a herringbone structure and lies flat on EG.[25] In this article, we present an *in situ* low-temperature (77 K) high-resolution STM/STS and synchrotron photoemission spectroscopy (PES) study of self-assembled PTCDA on EG as well as on HOPG for comparison. The molecular arrangement, film growth mechanism, and the interfacial electronic interactions between PTCDA and EG/HOPG are discussed.

RESULTS AND DISCUSSION

Figure 1b is a representative STM image (80×80 nm^2, $V_T = 1.0$ V) taken from an

*Address correspondence to phycw@nus.edu.sg, phyweets@nus.edu.sg.

Received for review July 24, 2009 and accepted October 18, 2009.

Published online October 23, 2009. 10.1021/nn9008615 CCC: $40.75

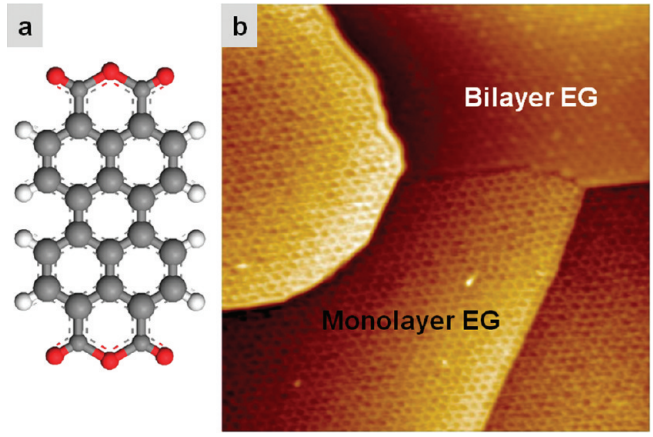

Figure 1. (a) Molecular structure of PTCDA, where the red, gray, and white spheres represent O, C and H atoms, respectively. (b) STM image (80 × 80 nm^2, V_T = 1.0 V) of ~1.3 monolayer EG grown on 6H-SiC(0001).

EG sample with thickness of ~1.3 monolayers and few defects. The surface is covered by either monolayer or bilayer graphene,[26] as labeled. At high bias voltage, the nanomesh[27] buffer layer underneath EG is more obvious in the monolayer regions. This nanomesh buffer layer forms prior to the development of single-crystalline graphene layers. Annealing SiC at ~1100 °C leads to the decomposition of SiC followed by the desorption of Si from the surface and an accumulation of carbon atoms to form a carbon-rich surface layer, referred to variously in the literature as the carbon nanomesh, interfacial graphene, or carbon buffer layer.[27−30] After annealing SiC substrates at 1200 °C or higher temperature, single-crystalline graphene films will grow on top of the interfacial graphene buffer layer.[26]

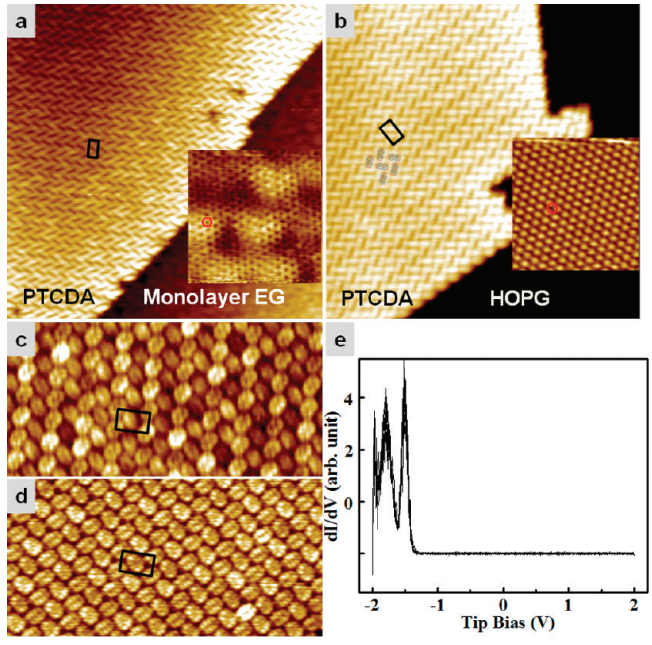

Figure 2. STM images of PTCDA monolayer on monolayer EG (a) (40 × 40 nm^2, V_T = −1.5 V) and on HOPG (b) (30 × 30 nm^2, V_T = −1.5 V). Six PTCDA molecules are imposed in panel b to guide the eyes. While the inset (5 × 5 nm^2, V_T = −0.1 V) in panel a shows the honeycomb structure of the uncovered monolayer EG, the inset (4 × 4 nm^2, V_T = 0.3 V) in panel b shows the atomic structure of HOPG. Panels c (20 × 10 nm^2, V_T = 2.5 V) and d (20 × 10 nm^2, V_T = 2.2 V) are the corresponding close-up at positive bias to show the arrangement of PTCDA on EG and on HOPG, respectively. The black rectangles in each panel mark the corresponding unit cells. (e) STS taken on PTCDA layer in panel a. Set-point: V_T = 1.5 V, I = 200 pA.

Figure 2a (40 × 40 nm^2, V_T = −1.5 V) and Figure 2b (30 × 30 nm^2, V_T = −1.5 V) are STM images of a well-ordered PTCDA island on monolayer EG and on HOPG, respectively. Six PTCDA molecules are imposed in Figure 2b to guide the eyes. The honeycomb structures of the uncovered EG and the atomic structure of HOPG are highlighted in the corresponding high-resolution STM inset (5 × 5 nm^2, V_T = −0.1 V) in Figure 2a and the inset (4 × 4 nm^2, V_T = 0.3 V) in Figure 2b, respectively. Figure 2c (20 × 10 nm^2, V_T = 2.5 V) and Figure 2d (20 × 10 nm^2, V_T = 2.2 V) are the corresponding close-up STM images of PTCDA on monolayer EG and on HOPG at positive tip bias. Due to the corrugation of the underlying nanomesh, the PTCDA film on monolayer EG appears less uniform than that on HOPG. On both surfaces, PTCDA molecules form similar herringbone assemblies. This herringbone packing structure is universal for PTCDA on surfaces such as Ag(111)[16] and KBr[20] and is attributed to attractive intermolecular interactions *via* C−H···O−C bonds.[31] The unit cells marked by black rectangles are similar in size, 2.15 × 1.05 nm^2, consistent with previous results on HOPG.[18,19] It is obvious that the PTCDA molecules lie flat on the graphene substrate with their molecular π-planes parallel to the surface, due to interfacial π−π interactions between PTCDA and EG[12,13] and the attractive intermolecular interactions *via* C−H···O−C bonds.[31] The observed flat-lying herringbone arrangement is different from the nonplanar adsorption geometry in a brick-wall structure reported in ref 24, which is apparently a low-temperature (4.7 K) phase for PTCDA on EG.

STS measurements were carried out to identify the local electronic properties of PTCDA on monolayer EG, with the tip bias fixed at 1.5 V and the set-point current at 200 pA. The differential tunneling conductance (dI/dV) as a function of the tip bias V, which is correlated to the electronic density of states of the sample, was obtained numerically from the I−V curve. Figure 2e shows the superposition of several dI/dV curves taken at random locations on the PTCDA monolayer shown in Figure 2a. Each curve was averaged over 10 spectra taken at one point. These curves reproducibly reveal two peaks at −1.52 and −1.78 V (tip bias), attributed to the LUMO and LUMO+1 of PTCDA, respectively. There are no other features in the bias window from −1.3 to 2.0 V, corresponding to the expected semiconductor behavior of the organic layer. The STS results are similar to previous STS measurements on multilayer PTCDA on an inert surface, Au(111),[21,22] where the LUMO is close to 1.4 eV (sample bias) and the gap is larger than 3.3 eV, suggesting that PTCDA intermolecular interac-

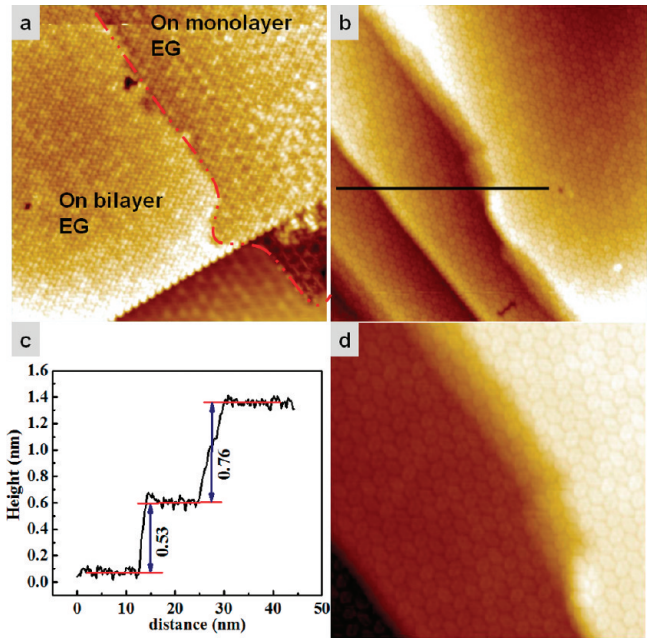

Figure 3. PTCDA follows EG continuously over two kinds of steps: (a) steps between monolayer and bilayer EG (50 × 50 nm², V_T = 1.5 V), (b) multiple SiC bilayer steps (50 × 50 nm², V_T = 1.5 V); (c) the corresponding line profile taken along the black line in panel b shows the step height; and (d) a close-up (25 × 25 nm², V_T = 1.5 V) to show the PTCDA continuously over multiple SiC bilayer steps clearly.

tions are much stronger than PTCDA−EG interfacial interactions. However, the STS spectrum of PTCDA on EG at 77 K in our experiment is slightly different from that measured at 300 K in ref 25. This difference may arise from temperature-dependent bonding geometry of PTCDA on EG, which can modify the electronic structure of PTCDA films. Further experiments of temperature-dependent STM, STS, and PES measurements of PTCDA on EG are needed to clarify this hypothesis. The observed STS results suggest that the electronic structure of PTCDA is decoupled from that of the underlying EG, implying very weak electronic coupling between PTCDA and EG, in good agreement with ref 25.

Figure 3a (50 × 50 nm², V_T = 1.5 V) and Figure 3b (50 × 50 nm², V_T = 1.5 V) are STM images showing the EG surface covered by monolayer PTCDA. In Figure 3a, bilayer EG is on the lower-left region and monolayer EG is on the upper-right region.[26] The boundary between them is highlighted by a red dotted curve. The PTCDA monolayer preserves its structural continuity across the steps between monolayer and bilayer EG. Figure 3b displays three terraces separated by one two-SiC-bilayer step (~0.53 nm in height) and one three-SiC-bilayer step (~0.76 nm in height), as illustrated by the line profile in Figure 3c taken from the black line in Figure 3b. The molecularly resolved STM image reveals that the PTCDA molecules retain their herringbone-like arrangement over these steps, as shown in the close-up in Figure 3d (25 × 25 nm², V_T = 1.5 V). Here we speculate that PTCDA follows the structure of graphene to form carpet-like film continuously over step edges, consistent with ref 25. The PTCDA film is not hampered by step edges in the saturated monolayer region.

Figure 4a (40 × 40 nm², V_T = −2.2 V) shows ~1.4 monolayer PTCDA on the EG surface. The PTCDA molecules in the second layer also display a herringbone arrangement that is continuous over a mono-SiC-bilayer step as noted by the red dotted curve. Figure 4b (250 × 250 nm², V_T = 2.5 V) displays a HOPG surface covered by ~1.1 monolayer PTCDA. On the upper half, there are two islands. The one on the left-hand side highlighted by a green dotted curve is the second layer PTCDA; the other one highlighted by a red dotted curve is monolayer PTCDA on another HOPG terrace one atomic layer higher. The image shows that the second layer PTCDA does not grow across the monatomic step edge of HOPG. Unlike EG, which grows continuously over SiC steps, the HOPG terraces are discontinuous over step edges.

Figure 5a (100 × 100 nm², V_T = −2.4 V) displays multilayer (>3 monolayer) PTCDA on the EG surface. The dislocation feature indi-

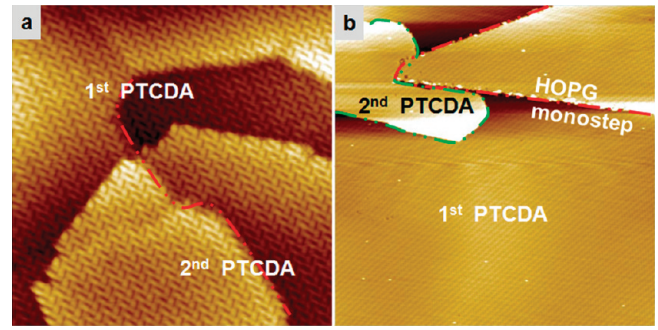

Figure 4. (a) STM image (40 × 40 nm², V_T = −2.2 V) showing 1.4 monolayer PTCDA on EG, with the first and second layer PTCDA forming continuously over single SiC bilayer steps highlighted by the red dotted curve. (b) STM image (250 × 250 nm², V_T = 2.5 V) of 1.1 monolayer PTCDA on HOPG, where the red dotted curve highlights the monostep of HOPG, and the green dotted curve highlights the boundary of the second layer PTCDA island.

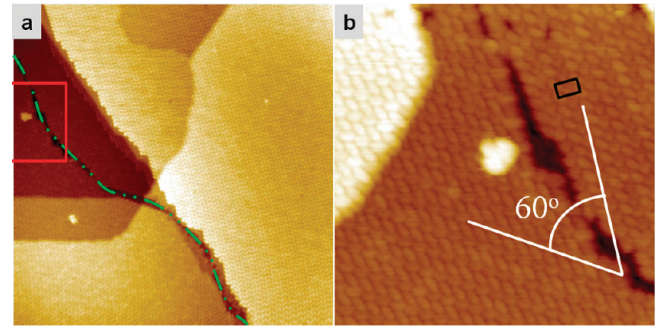

Figure 5. STM images of multilayer PTCDA on EG showing two equivalent PTCDA domains: (a) large-scale (100 × 100 nm², V_T = −2.4 V) and (b) close-up (30 × 30 nm², V_T = 2.6 V).

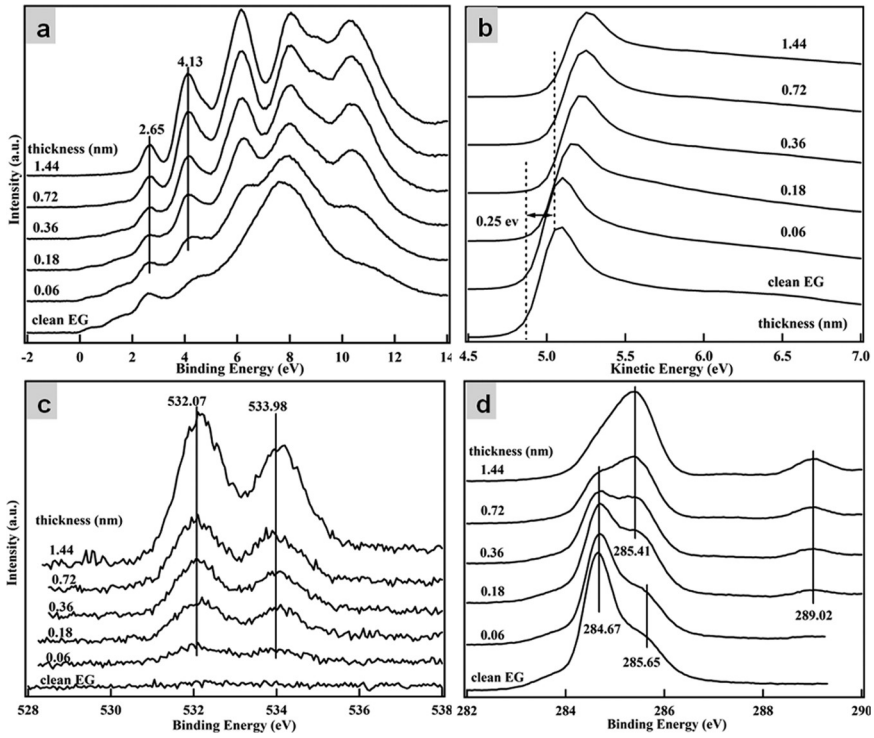

Figure 6. Synchrotron-based high-resolution PES spectra as a function of PTCDA thickness: (a) valence band spectra at the low binding energy part; (b) PES spectra at the low kinetic energy part (second electron cut off); (c) O1s core-level spectra and (d) C1s core-level spectra.

cated by the green dotted curve separates two PTCDA domains. Figure 5b (30 × 30 nm^2, V_T = 2.6 V) is a close-up taken from the red square in Figure 5a, showing all the PTCDA molecules in herringbone arrangement. The unit cell, marked by a black rectangle in Figure 5b, is the same size as that of the first PTCDA layer, suggesting a layer-by-layer growth mode. The angle between the two domains was measured to be 60 ± 1° as marked in Figure 5b, in agreement with PTCDA on HOPG.[32,33] This is attributed to the three-fold symmetry of the substrate. Because PTCDA is stable in air,[23] atomic force microscopy (AFM) experiments on the same surface were performed in ambient at room temperature. The AFM results (not shown here) reveal that the morphology of the PTCDA thin films follows that of EG.

We also carried out synchrotron-based high-resolution PES to investigate the electronic structure at the interface between PTCDA and EG. In Figures 6a and 6b representative PES spectra at the low binding energy region and the low kinetic energy region are shown as a function of PTCDA thickness, respectively. To resolve the low kinetic energy cutoff, a negative 5 V sample bias was applied. The vacuum levels (E_{vac}) were measured by linear extrapolation of the low kinetic energy onset (secondary electron cutoff) of the PES spectra. The bottom spectrum in Figure 6a displays the electronic structure of a clean EG/SiC surface with a main peak at ~7.6 eV and a weaker peak at ~2.5 eV, consistent with our previously reported results.[11] Upon 0.72 nm PTCDA deposition, the vacuum level was observed to shift upward by 0.25 ± 0.05 eV, as shown in Figure 6b. For such a noninteractive interface, this suggests a weak charge transfer taking place at the interface involving electron transfer from EG to the PTCDA layer. The highest-occupied molecular orbital (HOMO) peak of PTCDA is observed at the binding energy of 2.65 ± 0.05 eV, confirming the absence of features between 0 and 2 V in STS. Upon increasing the PTCDA coverage to 1.44 nm, the representative valence band spectrum of bulk PTCDA is observed,[17] without any apparent contribution from the EG/SiC substrate. For the thickness-dependent PES measurements, we did not observe any new interface states, confirming the weak electronic coupling between PTCDA and EG.

This weak interfacial interaction is supported by core-level PES measurements. Figure 6c shows the O1s core level spectra as a function of PTCDA deposition. Photon energy of 650 eV was chosen here to enhance the surface sensitivity. The two peaks at 532.07 and 533.98 eV attributed to C═O and C−O−C bonds in PTCDA increase with increasing PTCDA thickness, without any additional O1s peak component due to interfacial interactions. Figure 6d shows the evolution of C1s peaks during PTCDA deposition, using photon energy of 350 eV for higher surface sensitivity. The bottom spectrum of clean EG displays a very strong peak at the binding energy of 284.67 eV and a weaker shoulder at higher binding energy of 285.65 eV, consistent with previous results on 1.3 monolayer EG.[34] As the PTCDA coverage increases, two new peaks appear at 285.41 and 289.02 eV, which are due to the C-ring and O═C−O bonds of PTCDA molecules, respectively. The EG C1s peaks are simply superimposed by the two PTCDA components. No binding energy shift or new peak due to strong interfacial interactions was observed, confirming the weak interactions between PTCDA and EG, consistent with above-mentioned STS results.[25]

CONCLUSION

We present an *in situ* low-temperature (77 K) high-resolution STM and synchrotron-based PES study of self-assembled PTCDA on EG as well as on HOPG. PTCDA molecules self-assemble into a stable, well-ordered monolayer with an in-plane herringbone arrangement and with their molecular planes parallel to both EG and HOPG surfaces. The growth of PTCDA on EG follows a layer-by-layer mode. Synchrotron PES reveals weak charge transfer and weak

interactions between PTCDA and EG. In particular, PTCDA films grow continuously crossing over the underlying EG step edges, but not on HOPG. This suggests that it is possible to grow a pinhole-free PTCDA monolayer on EG. It is important for the functionalization of the EG surface using PTCDA derivatives to enhance the adhesion of a gate dielectric layer on EG, facilitating the growth of defect-free ultrathin dielectric layers in graphene-based electronic devices.

EXPERIMENTAL SECTION

All of the experiments were carried out on two ultrahigh vacuum (UHV) systems with base pressures lower than 2×10^{-10} mbar. Epitaxial graphene (EG) films were prepared by annealing chemically etched (10% HF solution) n-type Si-terminated 6H-SiC(0001) samples (CREE Inc.) in the multichamber endstation of the Surface, Interface and Nanostructure Science (SINS) beamline, Singapore Synchrotron Light Source,[35] where *in situ* synchrotron-based photoemission experiments were performed. The detailed sample preparation method could be found elsewhere.[26,27] The *in situ* LT-STM experiments were carried out in a custom-built multichamber system housing an Omicron LT-STM. All STM images were recorded in constant current mode at 77 K using chemically etched tungsten (W) tips.

PTCDA (Sigma-Aldrich, 99.9%) molecules were deposited *in situ* from a Knudsen cell (MBE-Komponenten, Germany) onto EG and HOPG substrates at room temperature. During deposition, the pressure was always maintained below 5.0×10^{-10} mbar. The deposition rate was calibrated to be either 0.06 nm/min, measured using the attenuation of Au 4f photoemission peak on a reference Au(100) sample in SINS, or 0.1 ML/min (ML: monolayer, refers to the surface fully covered by flat-lying PTCDA molecules) using a quartz crystal microbalance (QCM) and STM in the LT-STM system.

Acknowledgment. We acknowledge the support from NRF-CRP Grant R-143-000-360-281 "Graphene and Related Materials and Devices", and the ARF Grants R-143-000-392-133 and R-144-000-192-116.

REFERENCES AND NOTES

1. Geim, A. K.; Novoselov, K. S. The Rise of Graphene. *Nat. Mater.* **2007**, *6*, 183–191.
2. Novoselov, K. S.; Geim, A. K.; Morozov, S. V.; Jiang, D.; Katsnelson, M. I.; Grigorieva, I. V.; Dubonos, S. V.; Firsov, A. A. Two-Dimensional Gas of Massless Dirac Fermions in Graphene. *Nature* **2005**, *438*, 197–200.
3. Du, X.; Skachko, I.; Barker, A.; Andrei, E. Y. Approaching Ballistic Transport in Suspended Graphene. *Nat. Nanotechnol.* **2008**, *3*, 491–495.
4. Berger, C.; Song, Z. M.; Li, X. B.; Ogbazghi, A. Y.; Dai, Z. T.; Marchenkov, A. N.; Conrad, E. H.; First, P. N.; de Heer, W. A. Ultrathin Epitaxial Graphite: 2D Electron Gas Properties and a Route toward Graphene-Based Nanoelectronics. *J. Phys. Chem. B* **2004**, *108*, 19912–19916.
5. Wu, Y. Q.; Ye, P. D.; Capano, M. A.; Xuan, Y.; Sui, Y.; Qi, M.; Cooper, J. A.; Shen, T.; Pandey, D.; Prakash, G.; *et al.* Top-Gated Graphene Field-Effect-Transistors Formed by Decomposition of SiC. *Appl. Phys. Lett.* **2008**, *92*, 092102-1–092102-3.
6. Moon, J. S.; Curtis, D.; Hu, M.; Wong, D.; McGuire, C.; Campbell, P. M.; Jernigan, G.; Tedesco, J. T.; VanMil, B.; Myers-Ward, R.; Eddy, C.; Gaskill, D. K. Epitaxial-Graphene RF Field-Effect Transistors on Si-Face 6H-SiC Substrates. *IEEE Electron Device Lett.* **2009**, *30*, 650–652.
7. Wang, X. R.; Li, X. L.; Zhang, L.; Yoon, Y.; Weber, P. K.; Wang, H. L.; Guo, J.; Dai, H. J. n-Doping of Graphene through Electrothermal Reactions with Ammonia. *Science* **2009**, *324*, 768–771.
8. Novoselov, K. S.; Geim, A. K.; Morozov, S. V.; Jiang, D.; Zhang, Y.; Dubonos, S. V.; Grigorieva, I. V.; Firsov, A. A. Electric Field Effect in Atomically Thin Carbon Films. *Science* **2004**, *306*, 666–669.
9. Schedin, F.; Geim, A. K.; Morozov, S. V.; Hill, E. W.; Blake, P.; Katsnelson, M. I.; Novoselov, K. S. Detection of Individual Gas Molecules Adsorbed on Graphene. *Nat. Mater.* **2007**, *6*, 652–655.
10. Gierz, I.; Riedl, C.; Starke, U.; Ast, C. R.; Kern, K. Atomic Hole Doping of Graphene. *Nano Lett.* **2008**, *8*, 4603–4067.
11. Chen, W.; Chen, S.; Qi, D. C.; Gao, X. Y.; Wee, A. T. S. Surface Transfer p-Type Doping of Expitaxial Graphene. *J. Am. Chem. Soc.* **2007**, *129*, 10418–10422.
12. Dong, X. C.; Fu, D. L.; Fang, W. J.; Shi, Y. M.; Chen, P.; Li, L. J. Doping Single-Layer Graphene with Aromatic Molecules. *Small* **2009**, *5*, 1422–1426.
13. Dong, X. C.; Shi, Y. M.; Zhao, Y.; Chen, D. M.; Ye, J.; Yao, Y. G.; Gao, F.; Ni, Z. H.; Yu, T.; Shen, Z. X.; *et al.* Symmetry Breaking of Graphene Monolayer by Molecular Decoration. *Phys. Rev. Lett.* **2009**, *102*, 135501-1–135501-4.
14. Wang, X. R.; Tabakman, S. M.; Dai, H. J. Atomic Layer Deposition of Metal Oxides on Pristine and Functionalized Graphene. *J. Am. Chem. Soc.* **2008**, *130*, 8152–8153.
15. Di, C. A.; Wei, D. C.; Yu, G.; Liu, Y. Q.; Guo, Y. L.; Zhu, D. B. Patterned Graphene as Source/Drain Electrodes for Bottom-Contact Organic Field-Effect Transistors. *Adv. Mater.* **2008**, *20*, 3289–3293.
16. Temirov, R.; Soubatch, S.; Luican, A.; Tautz, F. S. Free-Electron-like Dispersion in an Organic Monolayer Film on a Metal Substrate. *Nature* **2006**, *444*, 350–353.
17. Gustafsson, J. B.; Zhang, H. M.; Moons, E.; Johansson, L. S. O. Electron Spectroscopy Studies of PTCDA on Ag/Si(111)-Root3 × Root 3. *Phys. Rev. B* **2007**, *75*, 155413-1–155413-10.
18. Ludwig, C.; Gompf, B.; Glatz, W.; Petersen, J.; Eisenmenger, W.; Mobus, M.; Zimmermann, U.; Karl, N. Video-STM, LEED, and X-ray Diffraction Investigations of PTCDA on Graphite. *Z. Phys. B* **1992**, *86*, 397–404.
19. Ludwig, C.; Gompf, B.; Petersen, J.; Strohmaier, R.; Eisenmenger, W. STM Investigations of PTCDA and PTCDI on Graphite and MoS_2: A Systematic Study of Epitaxy and STM Image Contrast. *Z. Phys. B* **1994**, *93*, 365–373.
20. Dienel, T.; Loppacher, C.; Mannsfeld, S. C. B.; Forker, R.; Fritz, T. Growth-Mode-Induced Narrowing of Optical Spectra of an Organic Adlayer. *Adv. Mater.* **2008**, *20*, 959–963.
21. Nicoara, N.; Roman, E.; Gomez-Rodriguez, J. M.; Martin-Gago, J. A.; Mendez, J. Scanning Tunneling and Photoemission Spectroscopies at the PTCDA/Au(111) Interface. *Org. Electron.* **2006**, *7*, 287–294.
22. Tsiper, E. V.; Soos, Z. G.; Gao, W.; Kahn, A. Electronic Polarization at Surfaces and Thin Films of Organic Molecular Crystals: PTCDA. *Chem. Phys. Lett.* **2002**, *360*, 47–52.
23. Hoshino, A.; Isoda, S.; Kurata, H.; Kobayashi, K. Scanning Tunneling Microscope Contrast of Perylene-3,4,9,10-Tetracarboxylic-Dianhydride on Graphite and Its Application to the Study of Epitaxy. *J. Appl. Phys.* **1994**, *76*, 4113–4120.
24. Lauffer, P.; Emtsev, K. V.; Graupner, R.; Seyller, Th.; Ley, L. Molecular and Electronic Structure of PTCDA on Bilayer Graphene on SiC(0001) Studied with Scanning Tunneling Microscopy. *Phys. Status Solidi B* **2008**, *245*, 2064–2067.
25. Wang, Q. H.; Hersam, M. C. Room-Temperature Molecular-Resolution Characterization of Self-Assembled Organic Monolayers on Epitaxial Graphene. *Nat. Chem.* **2009**, *1*, 206–211.

26. Huang, H.; Chen, W.; Chen, S.; Wee, A. T. S. Bottom-Up Growth of Epitaxial Graphene on 6H-SiC(0001). *ACS Nano* **2008**, *2*, 2513–2518.
27. Chen, W.; Xu, H.; Liu, L.; Gao, X. Y.; Qi, D. C.; Peng, G. W.; Tan, S. C.; Feng, Y. P.; Loh, K. P.; Wee, A. T. S. Atomic Structure of the 6H-SiC(0001) Nanomesh. *Surf. Sci.* **2005**, *596*, 176–186.
28. Owman, F.; Martensson, P. The SiC(0001)6Root-3 × 6Root3 Reconstruction Studied with STM and LEED. *Surf. Sci.* **1996**, *369*, 126–136.
29. Riedl, C.; Starke, U.; Bernhardt, J.; Franke, M.; Heinz, K. Structural Properties of the Graphene-SiC(0001) Interface as a Key for the Preparation of Homogeneous Large-Terrace Graphene Surface. *Phys. Rev. B* **2007**, *76*, 245406.
30. Kim, S.; Ihm, J.; Choi, H. J.; Son, Y. W. Origin of Anomalous Electronic Structures of Epitaxial Graphene on Silicon Carbide. *Phys. Rev. Lett.* **2008**, *100*, 176802.
31. Chen, W.; Li, H.; Huang, H.; Fu, Y. X.; Zhang, H. L.; Ma, J.; Wee, A. T. S. Two-Dimensional Pentacene:3,4,9,10-Perylenetetracarboxylic Dianhydride Supramolecular Chiral Networks on Ag(111). *J. Am. Chem. Soc.* **2008**, *130*, 12285–12289.
32. Forrest, S. R.; Burrows, P. E.; Haskal, E. I.; So, F. F. Ultrahigh-Vacuum Quasiepitaxial Growth of Model van der Waals Thin Films. II. Experiment. *Phys. Rev. B* **1994**, *49*, 11309–11321.
33. Kendrick, C.; Kahn, A.; Forrest, S. R. STM Study of the Organic Semiconductor PTCDA on Highly-Oriented Pyrolytic Graphite. *Appl. Surf. Sci.* **1996**, *104/105*, 586–594.
34. Emtsev, K. V.; Speck, F.; Seyller, Th.; Ley, L.; Riley, J. D. Interaction, Growth, and Ordering of Epitaxial Graphene on SiC(0001) Surfaces: A Comparative Photoelectron Spectroscopy Study. *Phys. Rev. B* **2008**, *77*, 155303-1–155303-10.
35. Yu, X. J.; Wilhelmi, O.; Moser, H. O.; Vidyaraj, S. V.; Gao, X. Y.; Wee, A. T. S.; Nyunt, T.; Qian, H. J.; Zheng, H. W. New Soft X-ray Facility SINS for Surface and Nanoscale Science at SSLS. *J. Electron Spectrosc. Relat. Phenom.* **2005**, *144*, 1031–1034.